The Journal of Experimental Biology 210, 1092-1108
Published by The Company of Biologists 2007
doi:10.1242/jeb.02729

The extensor tibiae muscle of the stick insect: biomechanical properties of an insect walking leg muscle

Christoph Guschlbauer, Hans Scharstein and Ansgar Büschges*
Zoological Institute, University of Cologne, Weyertal 119, 50923 Cologne, Germany
*Author for correspondence (e-mail: Ansgar.Bueschges@uni-koeln.de)

Accepted 23 January 2007

Summary

We investigated the properties of the extensor tibiae muscle of the stick insect (*Carausius morosus*) middle leg. Muscle geometry of the middle leg was compared to that of the front and hind legs and to the flexor tibiae, respectively. The mean length of the extensor tibiae fibres is 1.41±0.23 mm and flexor fibres are 2.11±0.30 mm long. The change of fibre length with joint angle was measured and closely follows a cosine function. Its amplitude gives effective moment arm lengths of 0.28±0.02 mm for the extensor and 0.56±0.04 mm for the flexor. Resting extensor tibiae muscle passive tonic force increased from 2 to 5 mN in the maximum femur–tibia (FT)-joint working range when stretched by ramps.

Active muscle properties were measured with simultaneous activation (up to 200 pulses s^{-1}) of all three motoneurons innervating the extensor tibiae, because this reflects most closely physiological muscle activation during leg swing. The force–length relationship corresponds closely to the typical characteristic according to the sliding filament hypothesis: it has a plateau at medium fibre lengths, declines nearly linearly in force at both longer and shorter fibre lengths, and the muscle's working range lies in the short to medium fibre length range. Maximum contraction velocity showed a similar relationship. The force–velocity relationship was the traditional Hill curve hyperbola, but deviated from the hyperbolic shape in the region of maximum contraction force close to the isometric contraction.

Step-like changes in muscle length induced by loaded release experiments characterised the non-linear series elasticity as a quadratic spring.

Key words: pinnate insect muscle, muscle properties, contraction dynamics.

Introduction

When animals move, a neurally generated motor output activates the musculo-skeletal system. This precise motor action is determined by the active and passive biomechanical properties of the muscles. Depending on their contraction dynamics, muscles can respond to different temporal components of their neural inputs (e.g. Brezina et al., 2000; Ballantyne and Rathmayer, 1981; Bässler and Stein, 1996; Full, 1997; Josephson, 1993; Meyrand and Marder, 1991; Morris and Hooper, 1997) (reviewed in Hooper and Weaver, 2000; Morris et al., 2000). Understanding of how nervous systems generate motor behaviours requires investigation of muscle properties as well as neural activity. This is particularly important in complex motor systems that function *via* the concerted action of multiple muscle groups, e.g. for terrestrial locomotion. In these systems the mechanical arrangement and activation of muscles can make synergistic muscles perform different roles. In the cockroach, for example, one of the two leg extensor muscles acts as a motor and the other as a brake (Ahn and Full, 2002). For organisms in which the neural component is already quite well understood, detailed investigation of muscles will allow a better characterisation of the roles that neural and muscular properties play in movement generation. One such organism is the stick insect *Carausius morosus* (Büschges, 2005; Orlovsky et al., 1999).

Motor output of the stick insect leg muscle control system is the result of a complex interaction between local sensory feedback, central neural networks governing the individual leg joints, and coordinating signals between the legs (e.g. Bässler and Büschges, 1998; Büschges, 2005; Dürr et al., 2004). The femur–tibia (FT)-joint is the functional knee-joint of the insect leg, and detailed information has been gathered with respect to morphological organization (Bässler, 1967) and the motoneuronal innervation pattern of the muscles involved, the flexor and the extensor tibiae (Bässler et al., 1996; Bässler and Storrer, 1980; Debrodt and Bässler, 1989; Debrodt and Bässler, 1990). In addition, motor output during walking movements (Bässler, 1993; Büschges et al., 1994; Fischer et al., 2001) and some aspects of the neural control, including the activity of the central premotor networks (Bässler, 1993; Büschges, 1995; Büschges et al., 2004; Driesang and Büschges, 1996), are known. This information has been sufficient to successfully construct a neuro-mechanical simulation of the stepping stick insect (Ekeberg et al., 2004). However, the control of

movement amplitude, i.e. the activation level of leg motoneuron pools and muscles, is only poorly understood, partly because neural and muscular properties interact at this level in movement generation (Blickhan et al., 2003; Brezina and Weiss, 2000; Chiel and Beer, 1997). In order to address this issue, it is necessary to investigate how the detailed aspects of neural control, e.g. changes in motoneuron activity, affect muscle activation and movements generated thereby, and the general working range of the neuron-to-movement transformation for stick insect leg muscles. Given the well-known neural aspects of stick insect leg motor control, understanding of the FT-joint control would be greatly increased by a better understanding of the biomechanics of the joint's muscular system. It would be particularly interesting to understand the control of activation of this muscle, i.e. the properties of force production and contraction related to frequency in activity of the innervating tibial extensor motoneurons, including the single twitch to maximum force ratio.

The flexor and extensor tibiae muscles are pinnate, as is typical for arthropods, and control tibia movement for posture and locomotion (Bässler, 1983; Bässler, 1993). The fibres of the two leg muscles are innervated by multiple excitatory motoneurons; fast, semifast and slow motoneurons for the flexor tibiae and one fast (the FETi) and one slow motoneuron (the SETi) for the extensor tibiae (Bässler and Storrer, 1980). In addition, the extensor muscle fibres receive innervation from the common inhibitor (CI_1) motoneuron 1 (Bässler et al., 1996; Bässler and Stein, 1996; Bässler and Storrer, 1980) and muscle fibres of the flexor tibiae receive innervation from CI_2 and CI_3 (Debrodt and Bässler, 1990). In the extensor tibiae muscle there is a systematic proximal-to-distal shift between muscle fibres innervated by the FETi alone and those that are also innervated by SETi and CI_1. During walking in the stick insect middle leg, all three extensor motoneurons are activated maximally during leg swing (Büschges et al., 1994; Schmitz and Hassfeld, 1989). CI_1 activity switches off force production of dually innervated fibres (Bässler and Stein, 1996). Depending on the walking situation, e.g. when walking on a double treadwheel, extensor motoneurons, i.e. also FETi, can also be active during stance before the initiation of the swing phase, albeit at a reduced level (Büschges et al., 1994; Graham, 1985; Schmitz and Hassfeld, 1989).

In the present study we investigated the geometrical characteristics of the stick insect FT-joint and the static and dynamic properties of the two antagonistic tibial muscles, the extensor and flexor tibae, in the middle leg. Due to the small number of excitatory motoneurons innervating it, we decided to investigate the static and dynamic properties of force generation for the extensor muscle in more detail. We first focused on static properties, i.e. the length dependence of isometric force in the muscle. We then present data on the dynamic properties of the extensor muscle, including the relationship between contraction force and velocity (Hill curve), muscle series elasticity, and the dependence of the muscle parameters on stimulation frequency.

Materials and methods

Experiments were carried out on 102 adult female stick insects of the species *Carausius morosus* Br. from a colony maintained at the University of Cologne. 10 animals of the same size as used in the experiment had an average body length of 77.1±2.28 mm and average mass of 940±70 mg. All experiments were performed under daylight conditions and at room temperature (20–22°C).

Muscle and fibre length measurements

The extensor and flexor muscles were exposed for length measurements by cutting a small window into the proximal and distal part of the femur. Muscle length was calculated under the microscope by determining the distance from the insertion of the most proximal fibre to an orientation mark (Fig. 1, shown for the extensor tibiae) and adding the distance from this mark to the insertion of the most distal fibre into the tendon. The tibia was moved on a plastic goniometer from 30° to 180° and length measurements were taken in 10° intervals. We considered this range (150°) as the maximum working range of both tibial muscles (Storrer, 1976; Cruse and Bartling, 1995). 90° was defined as the FT-joint angle at which both muscles are at their resting length for the stick insect (Friedrich, 1932; Storrer, 1976) and for *Blaberus discoidalis* (Full et al., 1998; Ahn and Full, 2002). Fibre length measurements were performed on muscles fixed *in situ*, with the joint at the 90° position, using 2.5% glutaraldehyde in phosphate buffer, pH 7.4 (Watson and Pflüger, 1994). Fibres were pulled from the proximal and medial parts of the femur because in these locations both muscles are primarily innervated by fast motoneurons (Bässler et al., 1996; Debrodt, 1980).

Force experiments

Force measurements were made exclusively on the extensor tibiae muscle of the middle leg, because it is innervated by only three motoneurons (Bässler and Storrer, 1980), all of which have their axons in nerve nl3 [nomenclature according to Marquardt (Marquardt, 1940)]. In contrast, the flexor tibiae muscle is innervated by about 14 motoneurons running in nerve ncr (Storrer et al., 1986; Debrodt and Bässler, 1989; Gabriel et al., 2003), and extracellular stimulation of this muscle is complicated to achieve. All legs except one middle leg were cut at the level of the mid-coxa. The animal was treated in accordance with the established procedures and was fixed dorsal side up on a balsa wood platform so that the tibia of the remaining leg was suspended above the edge of the platform. Coxa, trochanter and femur were glued to the platform with dental cement (Protemp II, ESPE, Seefeld, Germany). The distal end of the femur was opened carefully to ensure that as many muscle fibres are left intact as possible. Muscle force was measured by inserting a hook-shaped insect pin through the cut end of the muscle tendon. The pin was connected to the lever arm of a servo motor, which is part of an Aurora dual-mode lever system 300 B (Aurora Scientific Inc., Ontario, Canada), and muscle length set to the desired value. We tuned the lever system so that length control was critically damped and

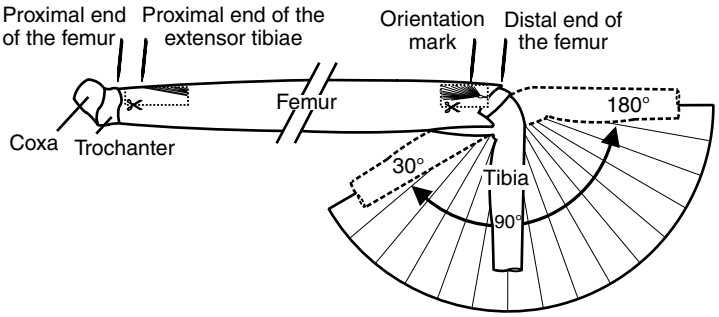

Fig. 1. Schematic representation of the geometrical arrangement of the femur–tibia joint in the stick insect middle leg. For details see text.

adjusted the inertia compensation to minimise force transients using triangle waveforms. The femoral cavity was filled with Ringer (NaCl 178.54 mmol l^{-1}, Hepes 10 mmol l^{-1}, $CaCl_2$ 7.51 mmol l^{-1}, KCl 17.61 mmol l^{-1}, $MgCl_2$ 25 mmol l^{-1}) (Weidler and Diecke, 1969) several times during the experiment. We did not study putative correlations between muscle performance and muscle mass, femur size, limb size or animal size.

Experiments to determine the active and passive force–length characteristics were carried out as follows: muscle length was manually set to a FT-joint angle of 90° at the beginning, our definition of the muscle's resting length (l_0). It was then released 0.75 mm (~0.5l_0) and subsequently stretched in coarse steps (mostly 0.15 mm) with sequencer-generated ramps of 0.05 mm s^{-1} up to 0.75 mm beyond the muscle's resting length (~1.5l_0). In some experiments we examined force development within the muscle's working range using small ramps (0.05 mm) within the range of ~0.8l_0 to ~1.2l_0 to obtain a more accurate screening. To investigate actively generated forces, the muscle was electrically stimulated with a paradigm of different stimulation frequencies at each length position after relaxation (for details, see Results, 'Passive muscle forces').

Force–velocity curves (Hill curves) were obtained according to established procedures. Extensor muscles were stimulated to reach 'steady-state' contraction under isometric conditions and then allowed to shorten under isotonic conditions against a variety of sequencer-generated counterforce levels. Muscle lengthening was accomplished by stretches while applying sequencer-generated load levels larger than the tetanical steady-state contraction force (for details, see Results, 'Dynamics of the muscle contraction').

Electrical stimulation of motor axons

The thorax was opened dorsally and the gut, fat and connective tissue removed to expose the mesothoracic ganglion. A bipolar hook electrode was then placed under nerve nl3 (Marquardt, 1940). The nerve was crushed proximally with a forceps and isolated with white vaseline (Engelhard Arzneimittel GmbH & CoKG, Niederdorfelden, Germany). To measure the tension generated by the middle leg extensor tibiae muscle, we electrically stimulated the axons of its innervating motoneurons, the FETi, SETi and CI_1. These axons have different diameters (Bässler and Storrer, 1980), so the three motoneurons can be sequentially activated by increasing stimulation strength; FETi has the lowest threshold (Fig. 2Ai,Aiv), SETi the next highest (Fig. 2Aii,Aiv), and CI_1 the highest (Fig. 2Aiii,Aiv). The determination of the appropriate current pulse amplitude to use in the nerve stimulation was complicated by a conflict between (1) the desire to routinely stimulate all three motoneurons (FETi, SETi and CI_1) and (2) the desire to keep the current amplitude low enough that the nerve could be repeatedly stimulated over long periods without damage. This issue was even more difficult to resolve because the dissection required to enable extracellular recordings from the extensor nerve F2 in the distal femur close to the muscle (necessary to test whether all three axons are being stimulated) inevitably damaged some more distal muscle fibres, which are mostly dually innervated (Bässler et al., 1996), and considerably lengthened the dissection procedure. It was consequently not possible both to perform the long experiments on undamaged muscles whose data are reported here in the Results, and to check if all three motor axons were being stimulated in the same preparation.

To overcome these difficulties, we performed 15 experiments with the dissection in which we were able to record extracellularly from the F2 nerve, and measured the relative thresholds of the three motor units. Since these experiments were short, we could also measure the force (due to the inevitable muscle fibre damage, in all cases less than the forces reported in the Results here) produced by the muscle as the number of stimulated nerve units changed. In five of these experiments stimulating the nerve at 1.5-fold the threshold (T) for visible twitches resulted in reliable stimulation of all three motor axons. In eight experiments, stimulation at this level was not sufficient to activate the two smaller fibres reliably (typically SETi but not CI_1 was reliably activated). However, increasing the stimulation amplitude in these experiments showed that when a sufficiently large stimulation amplitude was achieved to activate the other two units completely, negligible changes were induced (in seven preparations, none; in one, 3%) in muscle force production. Presumably this was because FETi induces by far the largest twitches, and because in most of these cases SETi was already being activated at the 1.5 stimulation level. Fig. 2Bi–iv shows forces and F2-recordings in response to a 50 Hz stimulation pulse train of a representative experiment. In Fig. 2Bi, 75% of the pulses excited FETi and 25% FETi and SETi. In Fig. 2Bii, 50% of the stimuli elicited FETi and 50% FETi, SETi and CI_1. Fig. 2Biii shows recruitment of all three motor units with every pulse, doubling the current amplitude in Fig. 2Biv shows no further increase in force. In the remaining two experiments, stimulating the additional two units resulted in an increase in muscle force of 20±4%. These experiments also showed that stimulating the motor nerve with current pulses 1.5 times larger than the visible twitch threshold for long periods of time did not induce any sign of nerve damage (e.g. an increase in stimulation failures).

These control experiments thus showed that in ~90% of preparations, stimulating nl3 with a current amplitude 1.5 times greater than the FETi threshold resulted in either activation of all three motor axons or, if not, that the failure to activate SETi and CI_1 completely had a negligible effect on muscle force production. In the remaining 10% of preparations, the lack of the SETi and CI_1 only induced a modest decrease in measured muscle force. We therefore chose to set the amplitude of the current pulses to approximately 50% above threshold generating a visible twitch (Malamud and Josephson, 1991). Pulse trains of different frequencies were applied using a SPIKE2 sequencer program at intervals of at least 30 s to allow return to the rest state. Pulse duration was 0.5 ms in all experiments (Josephson, 1985; Stevenson and Josephson, 1990; Malamud and Josephson, 1991; Full et al., 1998; Ahn and Full, 2002).

Data achievement and evaluation

Data were recorded on a PC using a MICRO1401 A/D converter with SPIKE2-software (both Cambridge Electronic Design Limited, Cambridge, UK). For isometric force experiments, the influence of filament overlap on force generation was examined by stretching the muscle in ramps of different size over a range of 1.5 mm using a SPIKE2 sequencer program. The stimulation protocol was carried out at each muscle length. In these experiments the dual-mode lever system was used exclusively as a force transducer. The stiffness of the measuring system was measured by connecting the insect pin directly to the base of the platform, and it was greater than 7500 mN mm^{-1}; it can therefore be neglected in our measurements [for a thorough discussion of the influence of the compliance of the measuring device, see Jewell and Wilkie (Jewell and Wilkie, 1958)]. Twitch kinetic measurements included the time to peak force (T_{max}), time to 50% relaxation (T_{50off}) and time to 90% relaxation (T_{90off}), all calculated relative to the force onset. For isotonic force experiments, the influence of load on contraction velocity and muscle series elasticity was determined by application of different force levels on the lever arm during tetanus using a SPIKE2 sequencer script. Custom SPIKE2 script programs were written for most of the data analysis. Plotting, curve fitting, and error evaluation were performed in ORIGIN (Microcal. Software Inc., Northampton, MA, USA).

Statistics

Mean values were compared using a modified *t*-test (Dixon and Massey, 1969). Means and samples were regarded as

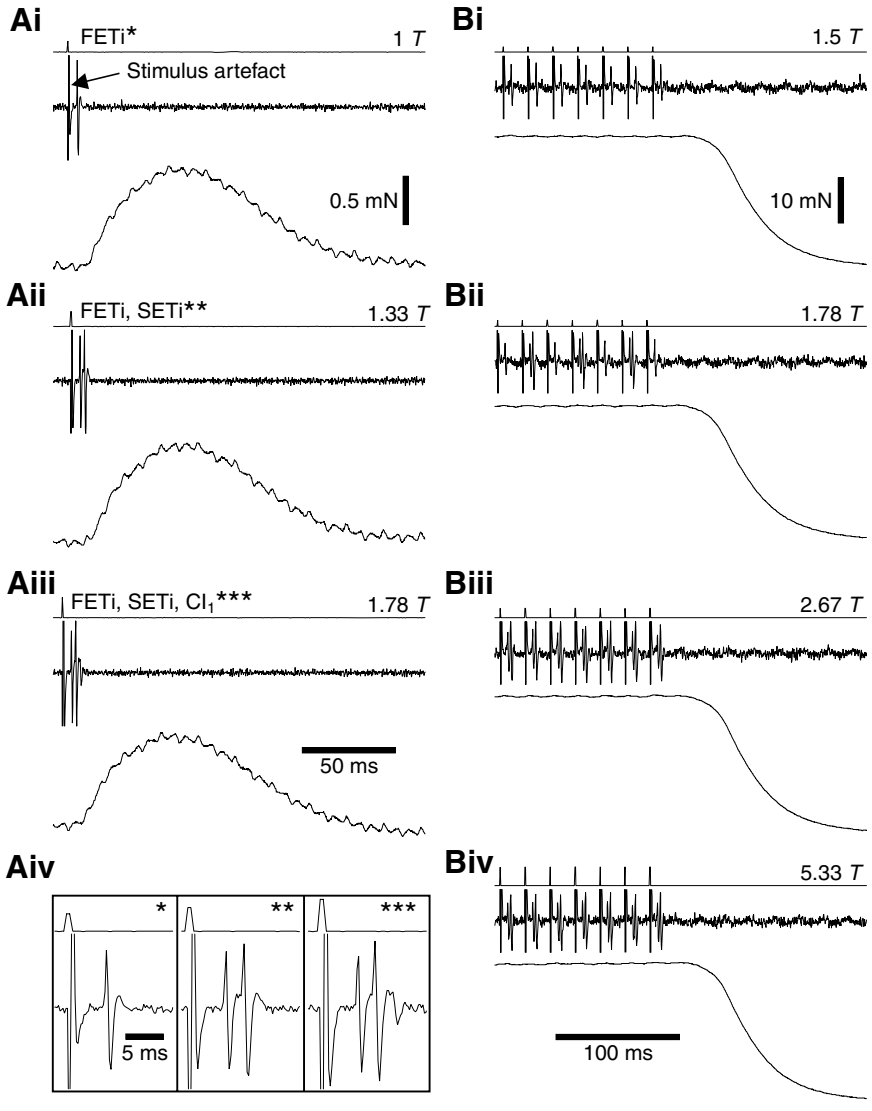

Fig. 2. Isometric forces induced in the middle leg extensor tibiae muscle by electrical stimulation of nerve nl3 with different current amplitudes. In all panels the top trace is a stimulus monitor (note pulse height changes as stimulus amplitude was increased), the second trace is an extracellular recording of nerve nl3, and the third trace is muscle force. (Ai–Aiii) Sequential recruitment of FETi (Ai), FETi and SETi (Aii) and FETi, SETi and CI_1 (Aiii) recorded in extensor leg nerve F2 in response to single stimuli. (Aiv) An enlarged version of the recordings, showing the sequential addition of new units (asterisks). 1 *T*=0.0023 mA. (Bi–Biv) F2-recordings and forces in response to a 50 Hz pulse train. (Bi) 75% of the pulses excited FETi and 25% FETi and SETi. (Bii) 50% of the stimuli elicited FETi and 50% FETi, SETi and CI_1. (Biii) Recruitment of all three motor units with every pulse. Doubling the current amplitude (Biv) induced no further increase in force. In this experiment the SETi spikes were of larger amplitude than FETi spikes. This is uncommon and likely because nerve F2 was recorded very distally in the femur. In all panels the electrical disturbance in the nerve recording that coincides with the stimulus is a stimulus artifact, not an action potential (arrow in Ai). *T*, threshold.

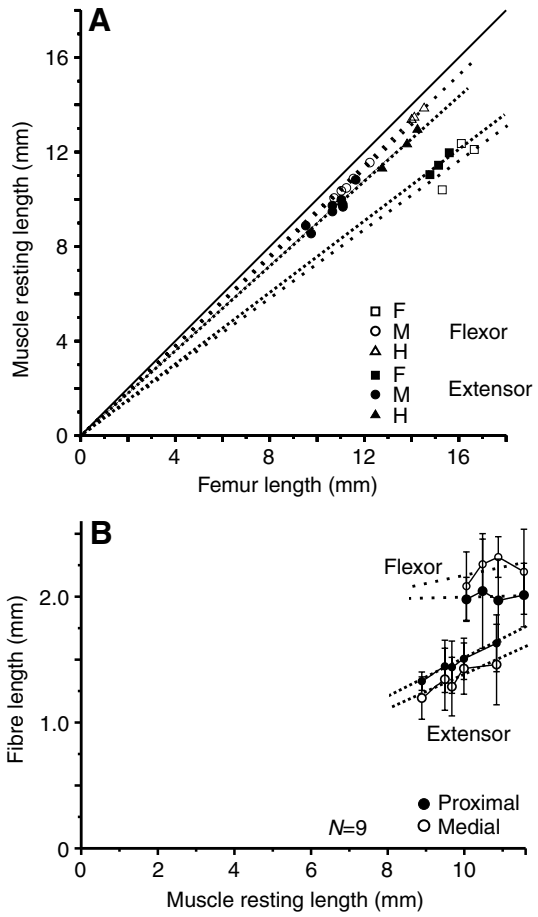

Fig. 3. (A) Relationship between muscle resting length and femur length in front leg (F; squares), middle leg (M; circles) and hind leg (H; triangles). Filled symbols, extensor tibiae; open symbols, flexor tibiae. The dotted lines give the linear fit under the assumption of pure proportionality between muscle length and femur length. The solid line indicates the 1:1 proportion, for comparison. Values are shown in Table 1. (B) Relation between middle leg muscle resting length and fibre length. Extensor muscle fibre length depends on resting muscle length (P<0.03), whereas no such dependence is present in the flexor muscle (dotted regression lines). Open, fibres in muscle medial regions; filled circles, fibres in muscle proximal regions. Values are means ± s.d. from nine experiments.

significantly different at P<0.05. The following symbols show the level of statistical significance: (–) not significant; *0.01<P<0.05; **0.001<P≤0.01; ***P≤0.001. In the text N gives the number of experiments or animals while n gives the sample size. All data were calculated as means ± s.d.

Results

Resting length, fibre length and cross-sectional area of tibial muscles

We first measured the resting muscle length (at 90° joint angle) of flexor and extensor tibiae for the front (flexor N=3, extensor N=3), middle (flexor N=5, extensor N=8) and hind legs (flexor N=3, extensor N=3, Fig. 3A). Linear regression of this data showed a significant dependence of muscle length on femur length (P<0.05 or better in five cases); only the flexor front leg data showed no significant dependence. Nevertheless we simplifed the dependence shown in Fig. 3A for all legs to a pure proportionality, forcing the regression lines through the origin (dotted lines, see also Table 1). For comparison the 1:1 proportion (solid line) is included. We next analysed the relation between fibre length and muscle length in the middle leg (Fig. 3B). Mean length of proximal fibres of the extensor tibiae muscle was 1.47±0.21 mm (N=5), which is about 0.13 mm longer than the medial muscle fibres (N=5). From these results, mean fibre length of the extensor muscle was 1.41±0.23 mm. In contrast, the mean length of flexor muscle proximal fibres was 2.0±0.32 mm (N=4), which is about 0.21 mm shorter than the medial fibres (N=4). From this, we calculated the mean fibre length of the flexor muscle as 2.11±0.30 mm. Regression analysis of this data showed a significant linear dependence of fibre length on extensor muscle length (P<0.05), whereas no such dependence was detected for flexor tibiae muscle fibres (see dotted regression lines).

Table 1. *Relationship between muscle length and femur length (see Fig. 3A)*

	Percentage of femur length	N
Extensor tibiae FL ■	75.7±1.0	3
Extensor tibiae ML ●	90.1±2.4	8
Extensor tibiae HL ▲	89.7±1.1	3
Flexor FL □	72.7±4.4	3
Flexor ML ○	94±0.5	5
Flexor HL △	95.4±0.1	3

FL, front legs; ML, middle legs; HL, hind legs.
Values are means ± s.d.

As for all orthopteran legs, both the extensor and flexor tibae of the stick insect are pinnate muscles (Storrer, 1976). This fibre arrangement markedly enhances effective muscle cross-sectional area and maximum muscle force (Hildebrand, 1988) but decreases effective muscle length and maximum contraction velocity. Given a mean fibre diameter of 0.125 mm (Bässler and Storrer, 1980), and a mean of 156 fibres per muscle (N=4; min. n=146, max. n=172), an estimated mean cross-sectional area of the extensor tibiae muscle is 1.9 mm^2. For pinnate muscles muscle length changes do not lead to the same changes in muscle fibre length; instead, muscle fibre length varies with muscle length times the cosine of the pinnation angle, which in turn varies as muscle length changes. For the extensor muscle, we calculated a range of angles from 8.2–12° for the proximal and 10.2–15.6° for the medial fibres within physiological muscle lengths. We ignored the cosine correction since it was only 3.7% for the largest angle (i.e. we treated the muscle fibres as though they were arranged parallel to the muscle longitudinal axis).

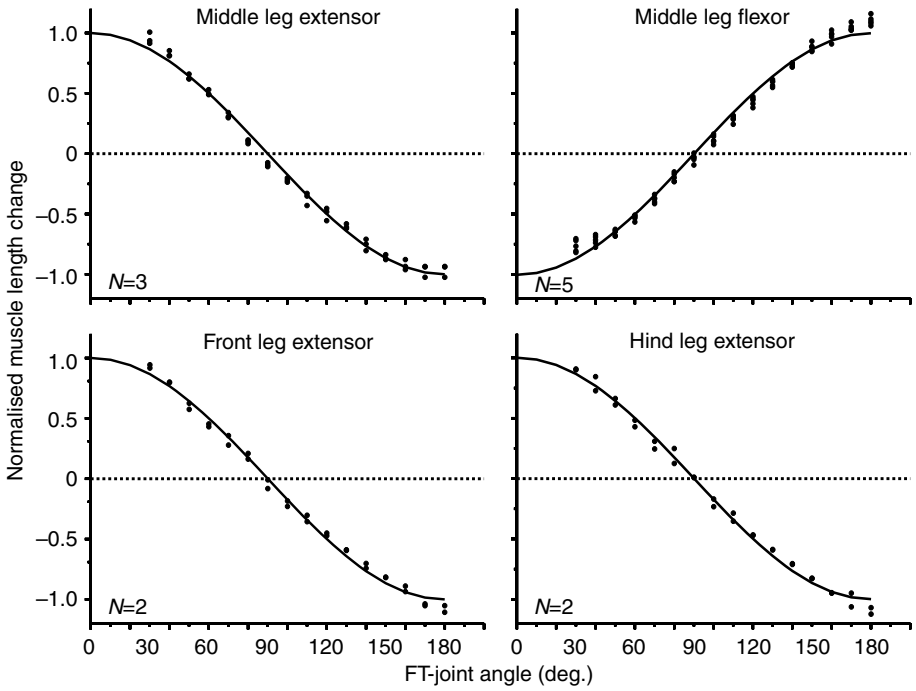

Fig. 4. Normalised muscle length change as a function of femur–tibia (FT)-joint angle. Extensor data are shown compared with +cos(α), flexor data are compared with –cos(α) (solid lines).

Relation between muscle length and joint angle and moment arms of muscles on the FT-joint

We measured the change in length of the tibial muscles as a function of FT-joint angle starting from the resting position of 90°. Given a fixed moment arm length of *H*, the length change should have the form of $x=H\cos\alpha$, where α is joint angle. Fig. 4 shows the normalised data compared to the cosine function. For the extensor muscle, changes in joint angle depend on +cosα, and for the flexor muscle on –cosα; this sign difference arises because extension shortens the extensor muscle and lengthens the flexor. The slope of plots of muscle length *versus* cosα is equivalent to the moment arm. Fig. 5 shows that the flexor muscle moment arms of all leg joints are about twice as long as the extensor muscle moment arms (mean flexor moment arm length, 0.56±0.04 mm, *N*=7, mean extensor moment arm length 0.28±0.02mm, *N*=7).

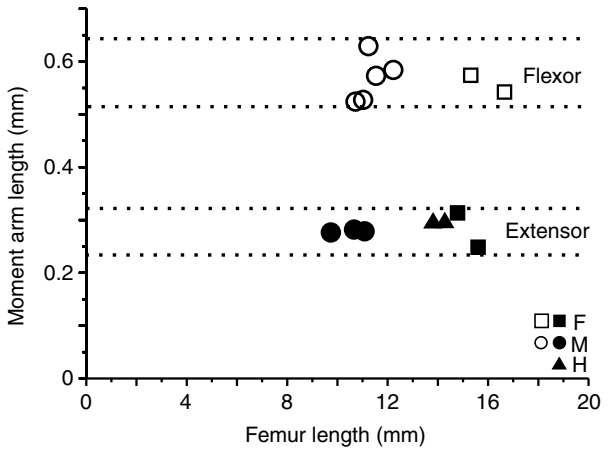

Fig. 5. Relation between femur–tibia joint moment arm and femur length. Note that moment arm does not depend on femur length. Closed symbols, data from extensor muscles from two front legs (F; squares), two hind legs (H; triangles), and three middle legs (M; circles); open symbols, data for flexor tibiae muscles from five middle legs (circles) and two front legs (triangles).

Isometric muscle forces

Passive muscle forces

The data presented up to now show how muscle length and muscle fibre length depend on FT-joint angle. We next turned to measuring passive and active muscle tension.

The resting (passive) tension of the middle leg extensor tibiae muscle was measured by lengthening the muscle with linear ramps (described in the Materials and methods), beginning at its most relaxed state. The resting tension of a stretched muscle exhibits a phase–tonic time course due to muscle visco-elastic properties (Fig. 6A) (Bässler, 1983; Malamud, 1988). We defined the amplitude of the phasic component of the response as the peak force induced by the stretch and, somewhat simplified (see Discussion), the tonic tension as the force at which the rate of change of force was smaller than ~0.3 mN min^{-1}. Both phasic- and tonic-component amplitude increased with increasing muscle stretch. Fig. 6B shows tonic force *versus* muscle length for nine extensor tibiae muscles and shows that passive tension increases from 0 mN at –0.75 mm to about 30 mN at +0.75 mm (0 mm=resting length). When leaving the innervation of the extensor tibiae muscle *via* nerve nl3 intact, passive tension was 2 mN higher as compared to the denervated situation (see Fig. 6B) throughout the muscle's working range (FT-joint angle between 30° and 180°, data not shown). An analysis of extensor muscle relaxation dynamics will be published elsewhere.

Forces of the activated muscle

We stimulated the three motoneurons with single pulses (Fig. 7A) and tonically at frequencies ranging from 10 Hz to 200 Hz (Fig. 7B; the maximum frequency of 200 Hz was chosen because this is in the range of maximum frequency generated by FETi during the swing phase of stepping movements). Single twitch had an average latency of 8.5±1.80 ms for all preparations (*N*=12). Note that the following times are measured relative to the force onset: maximum force was reached at T_{max}=26.41±6.30 ms (*N*=12). The subsequent reduction in muscle force to prestimulus levels

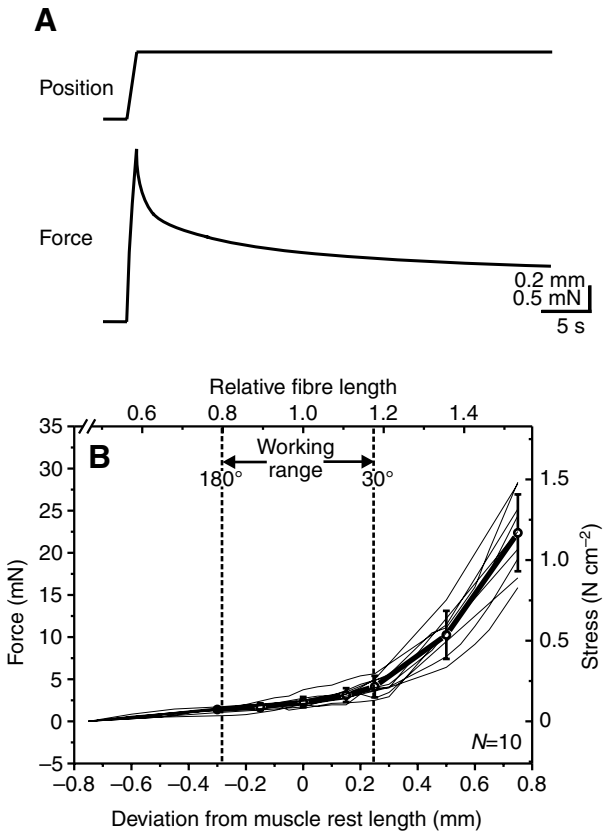

Fig. 6. Passive forces of the unstimulated, denervated middle leg extensor tibiae. (A) Time course of passive force induced by a ramp stretch of 0.5 mm amplitude in 1 s. Note the dynamic nature of the force change and its subsequent relaxation to a nearly constant value with maintained stretch. (B) Tonic resting force *versus* muscle length. Data from N=10 experiments (see text for details). Please note that the number for individual means can differ ($6 \leqslant N \leqslant 10$).

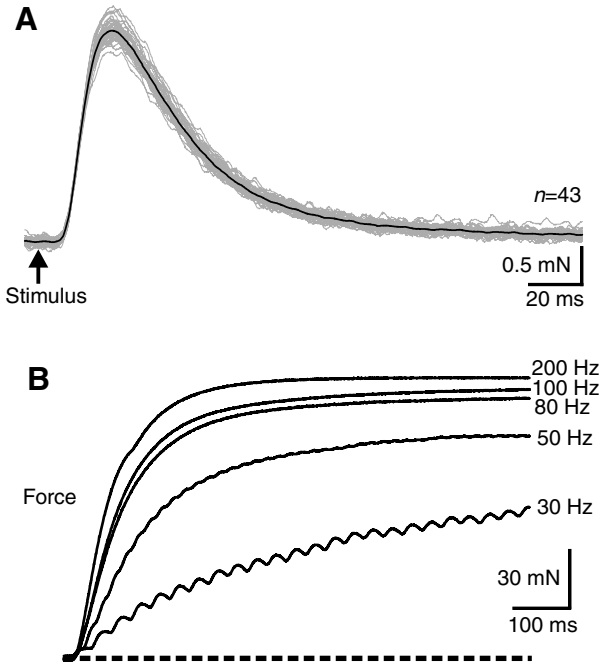

Fig. 7. (A) Average time course of a single twitch of the extensor tibiae (n=43). (B) Force development generated upon repetitive stimulation with differing stimulation frequencies between 30 Hz and 200 Hz (see values in Table 2). Broken line, resting force level.

took in general about 250 ms, with T_{50off} at 50% of the maximum force occurring at 60.69±15.65 ms (N=12). Force had declined by 90% (T_{90off}) after 149.89±67.93 ms (N=12).

At 30–50 Hz stimulation frequency, twitch contractions merged into an incomplete tetanus in all preparations (N=38; Table 2). The summated 'steady-state' force amplitude of the resulting contractions varied between preparations (see Table 3 and Fig. 8). At 80 Hz and higher stimulation frequencies, tetanus was complete in all preparations. At higher stimulation frequencies the force level only increased slightly with increasing stimulation frequency (Fig. 7B, Table 2), and was maximum with no further increase at 200 Hz. Maximum force values from nine preparations are given in Table 3.

Length dependence of contraction force

The isometric force generated by a muscle depends on the motoneuron firing rate and muscle length, because overlap of the filaments changes as muscle length changes (Rack and Westbury, 1969; Brown et al., 1999). We analysed the dependence of extensor tibiae muscle force upon these parameters by stimulating the muscle with single stimuli, intermediate frequency (10–80 Hz) and high frequency (200 Hz) tonic stimulations.

Fig. 8 shows (middle leg) extensor tibiae single twitch force, isometric force at 50 Hz stimulation frequency and at 200 Hz *versus* muscle fibre length. Besides the expected general length dependence on filament overlap (Gordon et al., 1966), the dependence of force generation on fibre length and stimulation frequency varied between experiments. In the single twitch measurements (Fig. 8A), maximum force varied eightfold (1.7–13 mN/0.09–0.68 N cm^{-2}); for the 50 Hz stimulation (Fig. 8B), fivefold (23.4–114.9 mN/1.22–6.00 N cm^{-2}); and for the 200 Hz stimulation (Fig. 8C), 2.7-fold (61.8–165.6 mN/3.23–8.65 N cm^{-2}) (see also Table 3).

Length dependencies at 200 Hz show maximum muscle force in the upper third of the working range, but curves with lower stimulation frequencies show a tendency to shift maximum force up to more elongated fibres (Fig. 8). This shift occurs in other muscles (Rack and Westbury, 1969; Brown et al., 1999), but it could vary between experiments; two examples with maximum and minimal frequency dependence of the length at which the muscle develops maximum force are shown in Fig. 9A,B.

Dynamics of the muscle contraction

The loaded release experiment

We have up to now described muscle activity under isometric steady state conditions. However in physiological conditions the muscle has to work under changing loads and changing lengths. It is thus essential to describe the muscle's

Table 2. *Tetanus/stress kinetics at different activation levels in a single animal (see Fig. 7B)*

Frequency (Hz)	P_0 (mN)/stress (N cm^{-2})	$t_{0.5P_0}$ (ms)	$t_{0.8P_0}$ (ms)
30	84/4.39	264	632
50	115/6.01	116	245
80	134/7.00	85	173
100	140/7.31	81	164
200	144/7.52	64	132

P_0, maximum isometric contraction force; $t_{0.5P_0}$ ($t_{0.8P_0}$), time to reach 0.5 (0.8) maximum force.

dynamic properties, both to understand its biological functions and to build predictive muscle models. 'Loaded-release' experiments are particularly useful for measuring these dynamic characteristics. In these experiments a muscle is stimulated to reach 'steady-state' contraction under isometric conditions and then allowed to shorten under isotonic conditions against a variety of counterforce levels. Fig. 10 shows an example of this experimental paradigm. The activated muscle responds to the switch to isotonic conditions (arrow in Fig. 10B) in two distinct phases: an abrupt initial shortening ('a'), followed by a subsequent smooth length change, in the case shown as a contraction ('b'). The first response is due to the series elastic properties of the muscle (Jewell and Wilkie, 1958), and considered later. The subsequent slow contraction, which is initially accompanied by some oscillations (Siebert et al., 2003; Edman, 1988; Edman and Curtin, 2001), is characterised by an almost linear initial time course followed by a late, saturating approach to its final length. The velocity of the linear phases of the contraction represents the maximum contraction velocity of the muscle for a given activation and load level (see the different traces in Fig. 10A). We chose a time span of 50 ms immediately after the end of the oscillations for calculating maximum contraction velocity; plotting this velocity *versus* the isotonic force level gives the muscle's force–velocity characteristic or Hill curve (Hill, 1938). The duration of the oscillations varied with the given load level and the stimulation frequency, and ranged from 17.4±4.16 ms for 30 Hz (N=5) up to 24.5±6.75 ms at 200 Hz (N=6).

The force–velocity relation and the Hill-hyperbola

Fig. 11A shows force–velocity data from seven experiments and fits of these data to the Hill hyperbola:

$$(V+b)*(P+a) = b*(P_0+a)\ , \qquad (1)$$

where V is velocity, P is force, P_0 is the isometric force just prior to the switch to isotonic conditions, and 'b' and 'a' the asymptotes (lying at negative values of P and V).

These data are clearly well fit by the hyperbola (mean R^2=0.996±0.006), but different muscles show considerable variation in P_0 and much less to V_0, the latter being the maximum contraction velocity without load. This variability can be overcome by normalising the Hill equation to P_0 and V_0:

$$(V/V_0+c)*(P/P_0+c) = c*(1+c)\ . \qquad (2)$$

This normalised version of the Hill-hyperbola gives a common value for the asymptotes c=b/V_0=a/P_0; the reciprocal value 1/c can serve as a measure for the curvature of the Hill hyperbola (Josephson, 1993). Table 4 gives the values V_0, P_0, c and R^2 for the measurements of Fig. 11A.

Deviations of the Hill curve from the hyperbolic shape

As reported by Edman et al. (Edman et al., 1976; Edman, 1988), we also find deviations of the Hill curve from the hyperbolic shape in the region of high forces (P near P_0) at low contraction velocities. The measured contraction velocities in this region lie systematically below the hyperbolic fit function. To demonstrate this, we took one example of the experiments in Fig. 11A and normalised the force values to P_0 (open circles in Fig. 11B). If we fit a hyperbola as before, but take only data below 0.65P_0, the resulting curve (solid line) shows the deviation of the measured velocities in the range >0.65P_0 from the hyperbolic fit.

This deviation persisted for values of P/P_0>1 (negative contraction velocities, i.e. stretch) (Edman et al., 1976; Edman, 1988). We therefore conducted a set of six similar experiments, changing from tetanical isometric contraction to loads higher than P_0, resulting in a 'loaded stretch', where the muscle is stretched with a certain force and stretch velocity is measured (Fig. 11B, filled circles to the right of P/P_0=1).

Table 3. *Variation of frequency-dependent maximum force/stress development in nine animals (see Fig. 8)*

	Force/stress (mN)/(N cm^{-2})		
	Single twitch	At 50 Hz	At 200 Hz
	–	43.7/2.28	84/4.39
	7.2/0.38	114.9/6.00	165.6/8.65
	13/0.68	57/2.98	61.8/3.23
	3.69/0.19	60.7/3.17	114.7/5.99
	4.65/0.24	76.6/4.00	87.2/4.56
	3.09/0.16	23.4/1.22	100.1/5.23
	2.06/0.11	50/2.61	143.4/7.49
	1.66/0.09	44.7/2.34	122.1/6.38
	10.55/0.55	111.7/5.84	147.1/7.69
Mean ± s.d.	5.74±4.15/0.3±0.22	64.74±31.04/3.38±1.62	114±33.96/5.96±1.77

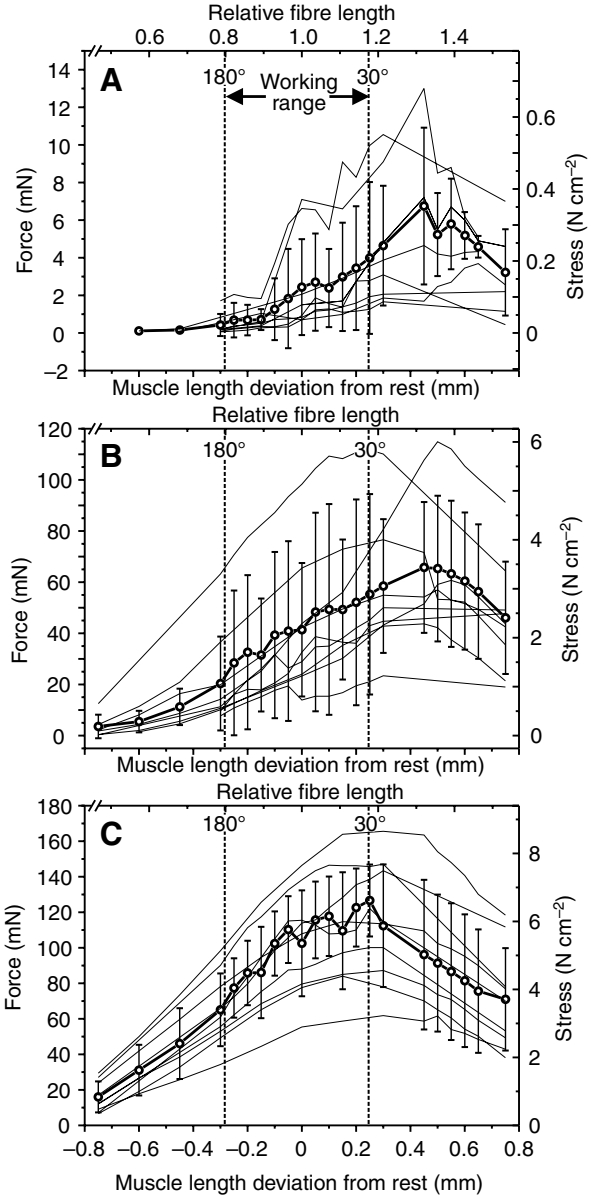

Fig. 8. Isometric force (mN, left ordinate) as a function of muscle stretch (mm, lower abscissa) and relative fibre length (top abscissa) in the middle leg extensor tibiae of nine individuals. Values for (A) single twitch (N=8), (B) 50 Hz (N=9) and (C) 200 Hz (N=9), see maximum values in Table 3. For comparison with other muscles, the right ordinate shows stress ($N\,cm^{-2}$). The working range from 180° (fully stretched joint angle) to 30° (maximally flexed joint angle) is marked. Please note that the number for individual means can differ; for single twitch measurements $3 \leqslant N \leqslant 9$, for 50 Hz and 200 Hz measurements $5 \leqslant N \leqslant 9$.

As maximum contraction velocity V_0 in all experiments did not scatter very much we found it reasonable to put the collected original velocity data as a function of P/P_0 in one diagram. The composite picture demonstrates that the Hill curve does not cross the abscissa with a non-zero slope (as the hyperbola would), but that the zero crossing is instead sigmoidal with an almost horizontal tangent.

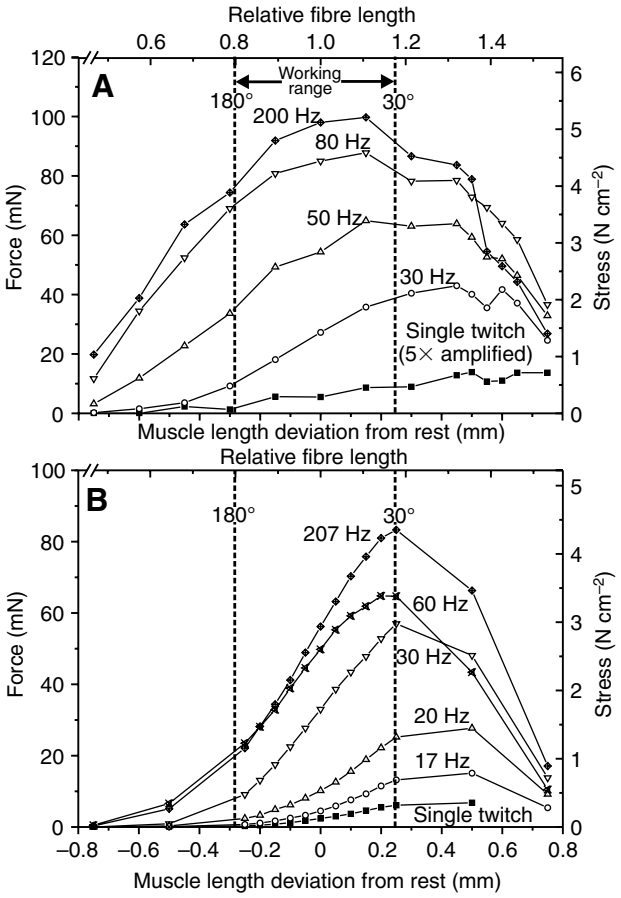

Fig. 9. Two extreme examples of extensor tibiae muscle single twitch and tetanical forces as a function of muscle stretch. With increasing stimulation frequency, the maximum force in A moves markedly towards lower values of fibre length while the shift in B is much less prominent. Axes as in Fig. 8.

Length dependence of V_0

Measuring the Hill curves at different muscle lengths and under minimal load reveals how maximum contraction velocity V_0 depends on muscle length. To investigate this issue we performed two experiments (Fig. 12), one experiment was done at 200 Hz and at 50 Hz stimulation frequency and with a rest load of 0.7 mN compared to a maximum isometric force of 69(35) mN at 200(50) Hz (filled symbols). The other experiment was done only at 200 Hz (open symbols) at a rest load of 4.5 mN compared with the maximum isometric force of 140 mN. Similar to the force–length characteristics (Fig. 8), the velocity–length curves showed a monotonic and nearly linear increase within the muscle's working range, followed by a plateau at longer fibre lengths.

Dependence of Hill curve parameters on stimulation frequency

Muscle activation is controlled by motoneuron spike frequency. We have investigated systematically how stimulation frequency influences the muscle Hill characteristic. Fig. 13 shows an example of the Hill curves

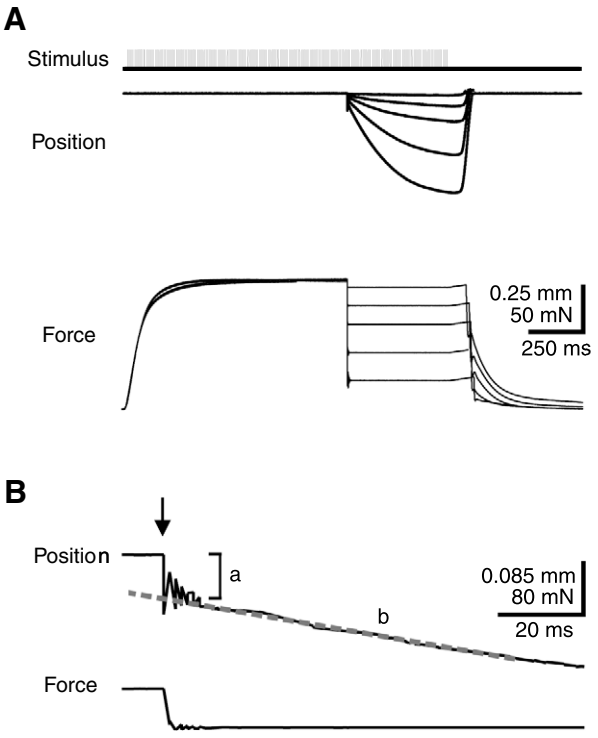

Fig. 10. The loaded release experiment. (A) Response of a tetanically activated muscle to a switch from isometric to isotonic conditions with counterforces less than the force the muscle had developed during its isometric contraction (see different 'Force' traces). (B) The muscle shows an abrupt length change (bracket 'a') followed by a smooth, initially linear contraction (b; see text for details).

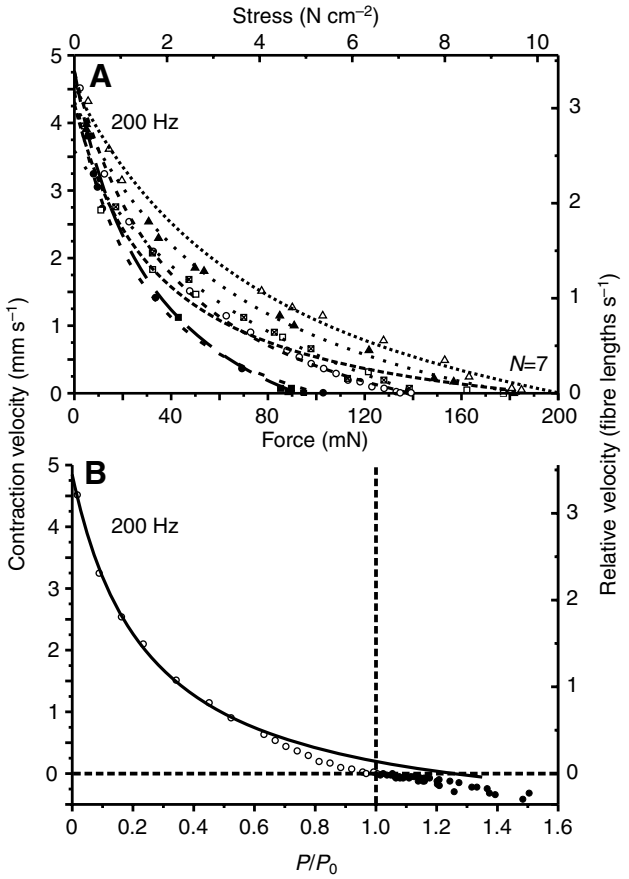

Fig. 11. (A) Variability of the force–velocity characteristic (Hill hyperbola, see Materials and methods for details) of the extensor muscle (see values in Table 4). Different symbols represent different animals. (B) Deviation of the force–velocity curve from hyperbolic shape in the region of P/P_0 between 0.6 and 1 for one typical experiment (open circles). In the region P/P_0>1, force–velocity measurements are shown under stretch (filled circles, data from six experiments) to demonstrate the sigmoid zero crossing of the Hill hyperbola. The force axis was normalised to the maximum isometric contraction force P_0. See text for details.

obtained from different stimulation frequencies. It is apparent that both V_0 and P_0 strongly increase with increased stimulation frequency (see also Table 5). Plotting P_0 *versus* stimulation frequency (Fig. 14A, N=11) for the different experiments reveals two main characteristics. First, P_0 shows a sharp increase at low frequencies between about 20 Hz and 80 Hz, and then saturates (reaches an unchanging maximum) at stimulation frequencies larger than 100 Hz. Second, the maximum saturated force at maximum stimulation frequency (in our case 200 Hz) varies from about 100 mN up to 190 mN in the different muscles. Fitting these data with an exponential saturation curve $P_0=P_{0max}(1-e^{-f/fo})$, in which P_{0max} is the saturation value and f_0 is the frequency at which the curve has reached 1–1/e of its saturation level, gave R^2=0.90±0.047 (min. 0.83, max. 0.98) and a mean f_0=56.6±17.2 Hz (N=11). The steepest and the shallowest fit to the data as well as the mean ± s.d. are added.

Plotting V_0 *versus* frequency can be fitted with a similar function and shows a nearly identical dependence with an even higher mean R^2=0.93±0.06 (min 0.86, max 0.98) and a similar mean f_0=57.7±17.9 Hz (Fig. 14B, N=5). Again the steepest and the shallowest fit as well as the mean ± s.d. are shown.

The paired data of V_0 and P_0 in the individual experiments in all cases showed a significant positive correlation (P<0.03, Fig. 14C, N=5). The V_0/P_0 ratios of the maximum values of V_0 and P_0 at 200 Hz correlate well with the slopes of the regression lines (P<0.05).

No correlation was found between the frequency constants f_0 of the corresponding P_0 and V_0 fits of the individual experiments, nor between the f_0 values and the P_0 and the V_0 values.

At present, a similar analysis is not possible for the curvature parameter 'c', mainly because we only gathered a limited number of values for 'c' in our experiments, since we looked for pairs of V_0 and P_0 and not for the complete Hill curve in most cases. However, the limited data do not show a systematic change of 'c' with stimulation frequency; the mean of the 14 'c' values we evaluated was 0.5±0.22.

Series elasticity and quadratic spring property of the activated extensor tibiae muscle

To analyse the series elasticity (spring constant) of the extensor tibiae muscle, we plotted the isotonic force change in

Table 4. *Maximum force/stress, maximum velocity, curvature and R^2 value of the Hill hyperbola at 200 Hz in seven animals (see Fig. 11A)*

	P_0 (mN)/stress (N cm^{-2})	V_0 (mm s^{-1})/(*FL* s^{-1})	*c*	R^2
	101.04/5.28	4.46/3.17	0.28	0.999
	92.54/4.83	4.77/3.39	0.36	1
	138.84/7.25	4.75/3.38	0.31	0.998
	194.41/10.16	4.28/3.04	0.18	0.983
	183.74/9.60	4.31/3.07	0.41	0.999
	201.62/10.53	4.56/3.24	0.44	0.995
	142.66/7.45	3.59/2.55	0.76	0.999
Mean ± s.d.	150.69±44.06/7.87±2.3	4.39±0.4/3.12±0.29	0.39±0.18	0.996±0.006

P_0, maximum isometric contraction force; V_0, maximum velocity; *c*, curvature; *FL*, fibre length.

the loaded release experiment (steps in the force trace in Fig. 10A) *versus* the associated fast initial length change (bracket at 'a' in Fig. 10B). In order to obtain a force–length characteristic comparable with similar measurements in the literature (Jewell and Wilkie, 1958) and with technical spring characteristics the data are presented in the following way (Fig. 15A): we plotted the independent, controlled force at the ordinate, the resultant length change on the abscissa. The origin length (0) for every set of data was the initial length of the isometric contracted muscle, and muscle shortening is thus plotted as negative values. The starting value of the force in each experiment is the tetanical isometric force at the given stimulation frequency. Each force step is plotted from this starting point, leading to a sequence of diminishing forces *versus* the ever more shortening length of the releasing muscle. Fig. 15A shows that the series elasticity of the extensor tibiae muscle is nonlinear and stiffness increases with increasing stretch. Consideration of these curves shows that the curve generated by 30 Hz stimulation, with its maximum force of 60 mN, has the same shape as the ⩽60 mN portions of the curves generated by the 50, 80 and 200 Hz stimuli. These data can therefore be combined by translocating the 30, 50 and 80 Hz curves to the left so they overlay the 200 Hz, maximum force curve [see also Jewell and Wilkie (Jewell and Wilkie, 1958) for further discussion of this issue]. When this is performed (Fig. 15B) all the force–length curves can be fitted by a single parabola $P(x)=\beta*x^2$ with β being the quadratic spring constant (for this experiment, β was 13900 mN mm^{-2}; maximum stiffness reached 3150 mN mm^{-1}). This procedure can be done with all series elasticity measurements at 200 Hz and led to an average β of 15000±2600 mN mm^{-2}; mean R^2=0.997±0.002 (*N*=5). It is currently unclear if the spring constant varies with muscle length.

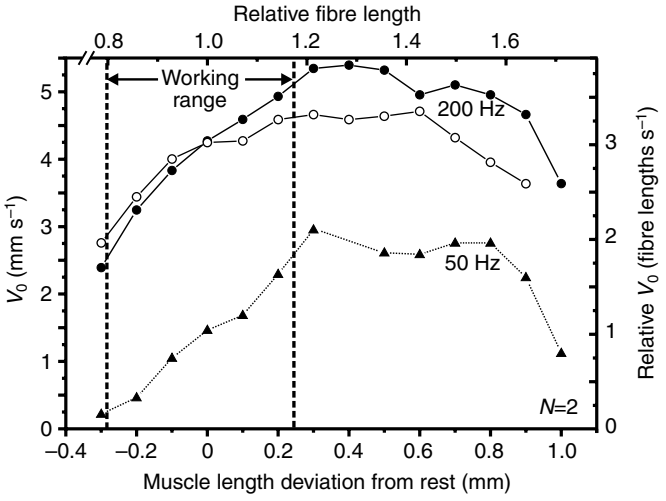

Fig. 12. Length dependence of maximum contraction velocity V_0 in two experiments. One experiment (filled symbols) was done at 200 Hz and at 50 Hz stimulation frequency. The other experiment (open symbols) was done only at 200 Hz (see text for details).

Discussion

Understanding the operation of a neuromuscular system requires investigating the system at both the neural and the muscular levels (e.g. Blickhan et al., 2003; Hooper and Weaver, 2000). We have investigated the extensor tibiae of

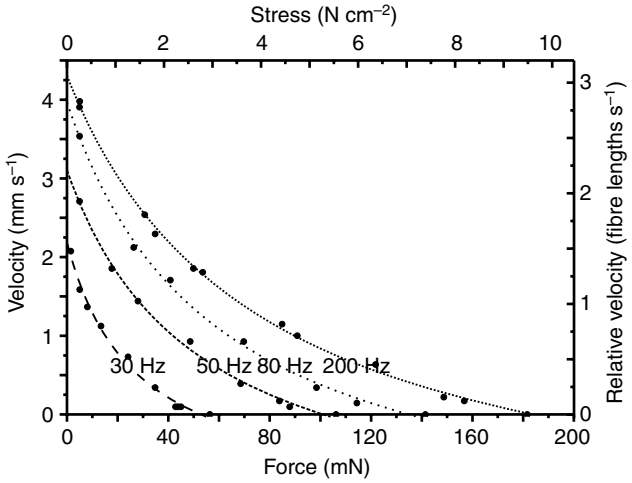

Fig. 13. Hill curves at different stimulation frequencies from one animal (see values in Table 5).

Table 5. *Maximum force/stress, maximum velocity, curvature and R^2 value of the Hill hyperbola at different activation levels in a single animal (see Fig. 13)*

Frequency (Hz)	P_0 (mN)/ stress (N cm^{-2})	V_0 (mm cm^{-1})/(FL s^{-1})	c	R^2
30	52.82/2.76	2.19/1.56	0.51	0.993
50	101.1/5.28	3.11/2.21	0.5	0.997
80	134.97/7.05	3.97/2.82	0.43	0.997
200	183.74/9.60	4.31/3.07	0.41	0.999

P_0, maximum isometric contraction force; V_0, maximum velocity; c, curvature; FL, fibre length.

the stick insect middle leg in great detail, because (i) the extensor tibiae muscle is a fairly simply innervated leg muscle with only two excitatory and one inhibitory motoneurons (Bässler and Storrer, 1980), (ii) its pattern of muscle fibre innervation and muscle fibre composition has been studied thoroughly (Bässler et al., 1996), and (iii) the activation of the motoneurons during active leg movements is known to some extent (Bässler and Büschges, 1998; Büschges, 2005). For example, when walking on a double treadwheel in late stance and during the initial part of the swing phase, as well as during the execution of compensatory leg reflexes, excitatory and inhibitory extensor motoneurons are activated together with instantaneous frequencies of up to 200 Hz (Büschges et al., 1994; Kittmann et al., 1996; Schmitz and Hassfeld, 1989). We therefore decided to stimulate the nerve with sufficient strength to activate all motoneurons in order to generate motoneuron activity resembling to some extent at least what is present in the swing phase of the stepping cycle. Although separate stimulation of the individual excitatory motoneurons is not possible due to FETi, SETi and CI_1 sending their axons through the same leg nerve (Bässler and Storrer, 1980), the mode of motoneuron activation, present in walking, can be mimicked by electrical stimulation of all three motoneurons at the same time. The extensor–tibiae system thus provides the opportunity to examine motoneuron output and muscular properties in a functional context. We have presented here a fairly complete picture of the geometry of the femur–tibia joint and the biomechanical properties of the extensor tibiae muscle. We will now discuss these data in terms of insect leg joint function and compare this system to previously analysed muscle–joint systems.

Geometry of the femur-tibia joint and tibial muscles

We found that the length of the flexor and extensor muscles of all three legs may be regarded as proportional to femur length. The tibial muscles of the middle legs and hind legs are 90–95% of the femur length, while for the front legs the proportion is only 73% (Fig. 3, Table 1). The latter is due to a specialized very narrow femur base in the front legs, that allows them to be held rostrally over the animal's head with virtually no angle of deviation from the animal's longitudinal axis, and thus to mimic twigs (Marquardt, 1940; Bässler, 1983). Due to this specialization there are no tibial muscle fibres present in the proximal 25% of front leg femurs.

Both femoral muscles are typical pinnate insect muscles. Due to this arrangement of the muscle fibres, their lengths are much shorter than muscle lengths (Fig. 3B). This almost parallel arrangement of many short muscle fibres, with one end attached at the inner cuticle and the other at the muscle tendon, markedly enhances the effective muscle cross-sectional area and the ability of the muscle (relative to muscle length) to generate force within a rigid, confined space (Full, 1997). For instance, the extensor tibiae muscle has an effective cross-sectional area of about 1.9 mm^2, while the inner lumen of the femur has a total cross-sectional area of only about 0.52 mm^2. This issue is even more important because the femur contains two tibial muscles, both the extensor and the flexor tibiae.

The relation between extensor and flexor tibial muscle length and the actual FT-joint angle (α), follows approximately a cosine function (Fig. 4). Importantly, cosine fit of muscle length over joint angle (Fig. 4) for the flexor muscle must not be exact. If it were, the torque of the flexor would become zero at the fully extended position of α=180°, and the muscle therefore would be unable to move the tibia out of this position. Therefore, we must assume that the fitted cosine function does not properly describe the range of angles close to the endpoint at 180°. Close inspection of the curves presented in Fig. 4 reveals that the muscle length does not reach the extended position at α=180° with a horizontal tangent, but rather that in this range of FT-joint angle the values still show a slope different from zero. It appears that the joint mechanics thereby avoid the problems of a mechanical dead point for the tibial muscles at extended joint angles. This also means that more detailed fits must be used to model joint geometry at maximum joint angles.

The flexor's moment arm being twice as long as the extensor's seems to be an adaptation to the flexor's longer fibres (see Fig. 3B) compared to those of the extensor (Fig. 5), leading to a similar relative length change of the muscle fibres during walking. This difference also has functional consequences: since the middle leg's flexor is mainly active during stance, a longer flexor moment arm would be an advantage for torque generation, whereas the extensor benefits from its shorter moment arm to manage fast movements during swing phase (Bässler and Büschges, 1998; Graham, 1985).

Muscle forces

Passive muscle force

All muscles exhibit dynamic forces against passive lengthening. The muscle's response to a step within the stretch

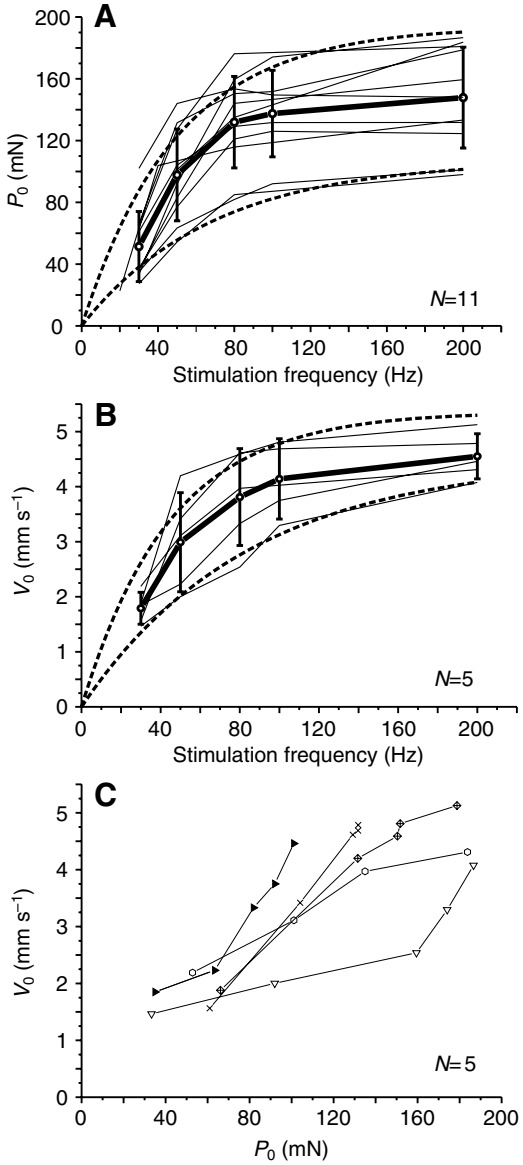

Fig. 14. Dependence of the parameters of the Hill curve on stimulation frequency. (A) Dependence of the isometric force P_0 on stimulation frequency (N=11). (B) Dependence of maximum contraction velocity V_0 on stimulation frequency (N=5). In both A and B the data from each experiment were fitted by an exponential saturation function leading to the same mean 'frequency-constant' of about 60 Hz for both dependencies. The dotted lines show the shallowest and steepest fits and the bold lines show mean ± s.d. Please note that the number for individual means can differ (in A, $6 \leqslant N \leqslant 9$; in B, $4 \leqslant N \leqslant 5$). (C) Coupling of maximum contraction velocity V_0 with isometric force P_0 under variation of stimulation frequencies (N=5). The values of each set of experiments are marked by connecting straight lines. For all individual experiments the data showed a significant correlation (P<0.03). Note that the maximum values V_0 and P_0 at 200 Hz for each experiment roughly determine the overall slopes of the diagrams. See text for details.

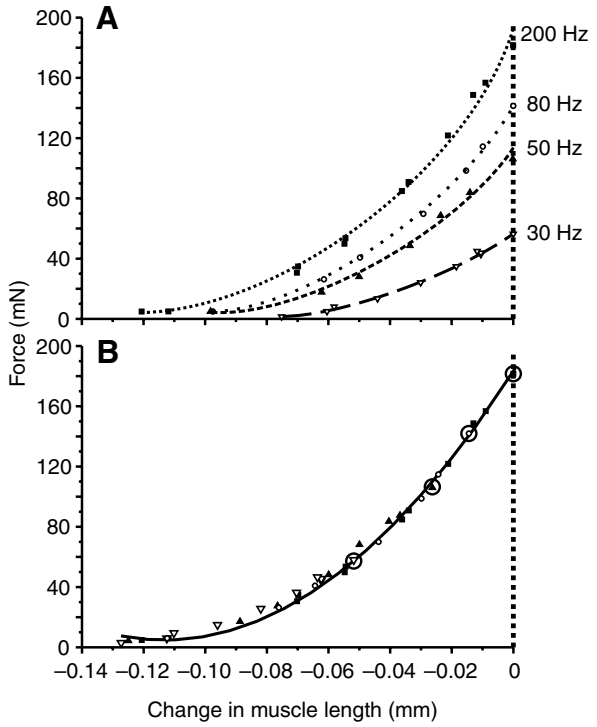

Fig. 15. Nonlinear spring-characteristic of the series elasticity. (A) Fast length change in the loaded release experiment starting from different tetanical force levels; change in force over the resultant change in length. (B) Common parabola fit for all shifted curves in A. The respective starting values are marked by circles. See text for details.

range has a power function characteristic (Thorson and Biedermann-Thorson, 1974). This means that stress relaxation becomes slower but will never reach a constant equilibrium (Malamud, 1989). This relaxation dynamic will be published elsewhere, so only a simplified description is provided here and we use the value of passive force after the rate of change, which was less than ~0.3 mN min^{-1}, as the static component. We show in the present work that the static portion of resting force in the extensor tibiae muscle increases almost exponentially with muscle length (Fig. 6). This systematic change in static resting tension is in good agreement with other muscles, e.g. the tergo-coxal flight muscle in *Schistocerca* (Malamud, 1989), the various extensors of the cockroach *Blaberus discoidalis* hind leg (Full and Ahn, 1995), as well as the feline hind limb muscle (Brown et al., 1999). However, comparison of the data presented here with those of other insect muscles shows that the resting tension of the extensor tibiae muscle is much weaker than in other systems. The maximum static resting force of the extensor tibiae is only about 20% of the active muscle force (maximum static resting tensions at 140% muscle length stay below 20 mN, whereas the muscle's maxium tetanical contraction force was as large as 150–200 mN), much lower than the values published (Malamud, 1989; Brown et al., 1999). The relative weakness of extensor muscle static resting force is even more striking when considered within the muscle's working range, where it does not exceed 5 mN. Of course, during walking it is not the static but the dynamic resistance to stretch that is likely of greatest functional importance. Fig. 5A

shows that the dynamic force component can be as much as twice the static component. None the less, our data suggest that passive resistance to stretch forces is likely to be much smaller than active forces (i.e. from the muscle's antagonist) at the femur–tibia joint.

Time course of single twitch and maximum tetanical forces

Single stimulation of the three motoneurons that innervate the extensor tibiae muscle generates a single twitch contraction, whose amplitude and time course can be compared with those in other insect muscles. First, the maximum force of the single twitch is only a few percent (ca 1%–10%) of the muscle's maximum force output (Table 3). This clearly differs from *Schistocerca* flight muscle Tcx_2 [in which single twitch amplitude is about 60% of maximum force (Malamud and Josephson, 1991)] and cockroach leg extensor muscle 177c (27%), whereas another leg extensor muscle 179 of the same animal (both 2%) lies within the range of our results (Ahn and Full, 2002).

The time course of the single twitch contraction (Fig. 7A) is much slower than that of the flight muscle from *Schistocerca* (Malamud and Josephson, 1991) and the flight muscles of *Manduca* (Stephenson and Josephson, 1990). The values for the extensors of the cockroach (Ahn and Full, 2002) and the front and middle leg extensors of the locust (Burns and Usherwood, 1978) are very similar to ours. Although the maximum tetanical force of the extensor tibiae is unexpectedly high (ranging from 80–200 mN), the normalized stress values (4.2–10.5 N cm^{-2}) are in the lower range of other insect muscles, much lower than e.g. the values for Tcx_2 (36 N cm^{-2}) of the locust or the leg muscles of the cockroach (25 and 47 N cm^{-2}) (Ahn and Full, 2002). Tettigoniid wing muscles [4–15 N cm^{-2} (Josephson, 1993)] lie within the range of our results.

Comparing our values with the middle and front leg extensors of the locust (Burns and Usherwood, 1978) reveals, surprisingly, that the absolute maximum force values of this 'normal' walking leg at 30–35 mN are much below the values for the stick insect. Unfortunately, we could not find published values for the effective cross-sectional areas of these muscles, so we cannot compare the values for maximum stress. Taken together, our results on the stick insect extensor muscle appear to be in good agreement with the expected requirements of a leg muscle in a slow walking and climbing insect: muscle forces reaching relatively high maximum values can be controlled by a broad range of motoneuron frequencies. The variability of muscle forces between different animals is discussed below.

Force–length characteristics

Due to the short length of pinnate muscle fibres, large length changes occur during contraction and relaxation. Therefore, it is particularly important to know the influence of fibre length on force in these muscles (cf. Gordon et al., 1966). Our data show that the extensor tibiae muscle shows a typical ascending-plateau-descending force *versus* muscle length relationship, that the muscle's working range lies on the ascending limb of this curve, and that considerable animal-to-animal variability exists with respect to the length and activation dependence of force production (Fig. 9, Table 3). A striking observation was the large change in force produced throughout the muscle working range, which sometimes showed a fourfold change in force as FT-joint angle changed from 30 to 180°, but generally resulted in a twofold change. An additional important point is that the muscle's maximum contraction force was normally generated in the upper third of its working range, thus the muscle was not generally exposed to any possible instabilities resulting from working with a non-monotonic force–length characteristic.

The dependence of maximum contraction force on fibre length at different activation levels is known from other muscles, for example feline SOL (Rack and Westbury, 1969), amphibian muscles (Stephenson and Wendt, 1984), and feline CF muscle (Brown et al., 1999). Two possible mechanisms have been proposed for this fact: length-dependent Ca^{2+}-release and length-dependent change of cross bridge attachment/detachment rate (Brown and Loeb, 1999). For the stick insect extensor tibiae, this particular muscle property is variable and does not correlate with the variation in maximum contraction force. Comparable insect muscle data are not known to us.

Dynamics of muscle contraction: loaded release and the Hill hyperbola

To evaluate the dependence of isotonic contraction velocity on load (Hill curve), we conducted a series of loaded release experiments (Fig. 10). Immediately after the transition from isometric to isotonic recording in these experiments contraction oscillations occurred (Fig. 10B). Such oscillations have been reported previously (Jewell and Wilkie, 1958; Edman, 1988; Edman and Curtin, 2001; Siebert et al., 2003) and may reflect the fast dynamic properties of the contractile mechanism under fast length change. After these oscillations we can measure the initial contraction velocity, which declines rather rapidly to zero (Fig. 10A). This is the result of the short fibre length and of the force–length characteristics of this muscle: by contracting, the muscle moves to a shorter length with reduced maximum force, which results in a reduced contraction velocity. The contraction stops when the maximum isometric force is equal to the load set in the experiment (see the different length traces in Fig. 10A). Furthermore contraction velocity is influenced directly by muscle length (see below).

The force–velocity curves derived from these data show the well-known hyperbolic shape of the Hill curve (Fig. 11A, Table 4). The maximum isometric contraction forces varied between 80 mN and 200 mN. The range of maximum contraction velocities was much narrower, 3.5–4.75 mm s^{-1}. Normalising the force to the effective cross-sectional area of 1.91 mm^2 resulted in tensions of 4.2–10.5 N cm^{-2}. Normalising contraction velocity to fibre length (*FL*=1.41 mm) gave relative contraction velocities ranging from 2.5 to 3.4 *FL* s^{-1}. Similar to the passive and active tension values reported earlier, these relative velocity values are located at the lower end of the

spectrum of data known for different muscles, again indicating that stick insect leg muscles are adapted to generate slow movements.

The Hill curve deviates from a hyperbola when contraction velocity is very small and muscle force is close to maximal (Edman et al., 1976; Edman et al., 1978). In our data as well (Fig. 11B), above force values of $0.65P_0$, the corresponding velocity values are markedly lower than those predicted by the hyperbolic fit. Altering the loaded release experiment to include negative contraction velocities (stretch) showed that these data cross zero with a slope near zero, which corresponds with Edman et al.'s findings for single muscle fibres (Edman et al., 1976; Edman et al., 1978). Edman explains the deviations in the high force region as a reduced contraction velocity. In contrast to this interpretation, we think that this deviation may result from an intrinsic Coulomb-friction in the muscle fibres. This would result in a reduced active contraction force and would produce the sigmoid zero crossing of the Hill curve when changing the direction of movement. This intrinsic friction would lead to high passive forces that would need to be overcome before movement could occur, when the tibia load changes, as for instance, at the transition from swing to stance in walking (Büschges et al., 1994; Fischer et al., 2001) or searching (Karg et al., 1991; Bässler, 1993).

Dynamics of muscle contraction: length dependence of contraction velocity

While the length dependence of contraction force was a direct indication for the sliding filament hypothesis (Gordon et al., 1966), the question of whether the contraction velocity also depends upon fibre length is not as straightforward. White treated the contraction velocity according to Gordon et al. (Gordon et al., 1966) as being independent of fibre length and coined the 'tug-of-war-concept': '*The tension such a team can exert is proportional to the number of members in that team, but if the rope between two teams is cut, then the maximum rate at which the team can move is the speed with which any individual member can run*' [(White, 1977), p. 46]. However, in doing so, White cited Gordon et al. incompletely: Gordon et al. stated for long fibre lengths beyond the resting length that V_0 changes only little (15%) with length, while isometric force P_0 declines from 100% to 40% (Gordon et al., 1966). Our data presented in Fig. 12 show a similar broad plateau, much broader than the narrow maximum of the force–length curves (Figs 8 and 9). But Gordon et al. show explicitly that for shorter fibre lengths the maximum contraction velocity V_0 decreases linearly with fibre length, in agreement with our findings depicted in Fig. 12. This has also been shown in other publications, e.g. Abbot and Wilkie (Abbot and Wilkie, 1953). Edman finds a similar result for short fibre lengths (Edman, 1979), but an increased V_0 in the range of long fibres, presumably caused by the increased resting tension of the fibres. Although it was not possible, with our experimental design, to measure the contraction velocity without any load, we tried to keep the residual load as small as possible. The residual load at 200 Hz accounts for 1% (filled circles) and 3% (open circles) of the maximum contraction force P_0 (the values of the rest load are not shown). Under these conditions, the contraction velocity decreases to 50% at short fibre lengths, whereby the relative load increases to 1.6% (5%) because of the decreasing maximum contraction force. Since this minor rise in the relative load is negligible, we can be sure that the shown length dependence is real.

The 50 Hz curve shows that an increase in relative load can indeed falsify the length dependence: here, the relative portion increases from 2% to 80% of the maximum contraction force. The contraction velocity falls back to almost zero, because the strongly reduced contraction force at this length has almost reached the force value of the residual load.

Variability of muscle forces and of the force–length dependence

The muscle forces measured show variation (Figs 8, 11A, Table 4). Maximum tetanical force at 200 Hz has a relative s.d. of ±29.8%, while the variability for lower stimulation frequencies, and especially for the single twitch force, is much higher. The range of maximum contraction velocities is rather narrow with (relative s.d. ±9.1%). Unfortunately we did not systematically record body size and mass, so we could not look for size-correlated influences. Examination of ten animals of the same body size and mass as those chosen for the experiments confirmed that size is unlikely to be a possible source of this variability: mean body length was L=77.1±2.28 mm, mean body mass M_b=940±70 mg, much less variation than one would expect for such a high variability of force. A systematic preparation error that might lead to a stronger variation in activation is also rather unlikely because (1) variation is higher for contraction forces and is lower for contraction velocities, and (2) this variation can be found in different sets of experiments (force–length characteristics, maximum contraction force depending on activation, force–velocity characteristics at 200 Hz) and its magnitude between the different sets is very comparable (see Tables 3 and 4, mean ± s.d. in Fig. 14). We therefore consider this variation to be a property of the extensor tibiae, and whether it applies to other stick insect muscles needs to be examined. Even more important is the fact that other insect leg muscles show considerable variability in contraction force, for example the extensor 117c in *Blaberus discoidalis* (Ahn and Full, 2002) or the pro- and mesothoracic extensor tibiae in *Schistocerca gregaria* (Burns and Usherwood, 1978). The relative standard deviations of force in the cockroach are ±38% at twitch, ±31% at tetanus, and in the locust, ±30% at twitch in response to prothoracic and ±48% in response to mesothoracic FETi stimulation. These values are in a similar range to ours (±72.3% at twitch, ±47.9% at 50 Hz stimulation and ±29.8% at 200 Hz stimulation).

Dynamics of muscle contraction: control of activation and series elasticity of the activated muscle

We investigated the dependence of the extensor tibiae Hill curves across a range of stimulation frequencies that covered

the physiological firing range (30–200 Hz) of the extensor motoneurons (Fig. 13). Both the maximum contraction force P_0 and the maximum contraction velocity V_0 greatly increased with frequencies up to around 60 Hz, and then began to level off, achieving near maximum values at frequency values beyond 100 Hz (Fig. 14A,B). Both data sets were well fit with equations of the form $P=P_{0max}*(1–e^{(–f/f0)})$ and $V=V_{0max}*(1–e^{(–f/f0)})$, in which the mean 'frequency constants' f_0 were identical. f_0 may reflect the time constant of a process common to both force production and contraction velocity such as Ca^{2+}-summation. Consistent with this common dependence, V_0 and P_0 were linearly correlated with each other in single preparations, although some animal-to-animal variability was present (Fig. 14C). In summary, these data suggest that for the control of force and contraction velocity of the extensor tibiae, changes in motoneuron firing are most effective below 80 Hz. We only measured the frequency-dependence of V_0 and P_0 and did not assess the length dependence of this curve, as has been done by others (Brown et al., 1999), or consider how maximum contraction velocity could be assessed using much higher stimulation frequencies [up to 400 Hz (De Haan, 1998)]. Similar to the parallel length dependence of V_0 and P_0 at shorter fibre lengths, our results show that for this muscle there is also a more or less parallel influence of excitation on V_0 and P_0 (Figs 13 and 14). Experiments where the force–velocity curves of *Schistocerca* flight muscles were measured at different times during a twitch provided similar results: both V_0 and P_0 changed similarly with excitation (Malamud and Josephson, 1991).

We evaluated the series elasticity of the extensor tibiae muscle by measuring the initial fast length change of the muscle upon switching to isotonic recording conditions (e.g. Fig. 15). The series elasticity was non-linear, with a quadratic force–length characteristic. The spring properties of the frog (*Rana temporaria*) sartorius were measured and fit the individual measurements with a composite curve with an exponential slope at low forces and an almost linear shape at higher forces (Wilkie, 1956; Jewell and Wilkie, 1958). In contrast to these data with a finite slope at low values, our curves reach the zero point with horizontal slope.

We have presented here data characterising the geometry of the femur–tibia joint and its muscles, force–length and force–velocity relationships of the extensor tibiae muscle, and frequency dependence of the muscle parameters. These data show that the extensor tibia muscles are weaker and slower than many comparable insect muscles, and are sufficient to begin modelling this muscle's activity. However, more complete understanding of its role in behaviour requires further experiments using physiological stimulation regimes (Hooper et al., 2006; Hooper et al., 2007) to investigate the interaction of muscle activation and the properties of the Hill hyperbola at high forces, and to consider the finding that contraction velocity depends on fibre length. Finally, one further important aspect still needing analysis is the influence of the release properties of the extensor muscle under counter-activation of the antagonist, i.e. the flexor tibiae.

We thank Drs V. Dürr, Ö. Ekeberg, R. J. Full, S. L. Hooper and K. G. Pearson for their valuable comments in the course of the work. We are grateful to U. Bässler, R. Blickhan, S. L. Hooper and two anonymous referees for their comments on the manuscript and thank S. Meyen-Southard for her help in editing the paper. The work was supported by DFG-grant Bu857/8, a grant from the Institute for Advanced Study in Berlin, the Boehringer-Ingelheim-Foundation and a travel grant from the province NRW.

References

Abbot, B. C. and Wilkie, D. R. (1953). The relation between velocity of shortening and the tension-length curve of skeletal muscle. *J. Physiol.* **120**, 214-223.

Ahn, A. N. and Full, R. J. (2002). A motor and a brake: two leg extensor muscles acting at the same joint manage energy differently in a running insect. *J. Exp. Biol.* **205**, 379-389.

Ballantyne, D. and Rathmayer, W. (1981). On the function of the common inhibitory neurone in the walking legs of the crab, *Eriphia spinifrons*. *J. Comp. Physiol.* **143**, 111-122.

Bässler, U. (1967). Zur Regelung der Stellung des Femur-Tibia-Gelenkes bei der Stabheuschrecke *Carausius morosus* in der Ruhe und im Lauf. *Kybernetik* **4**, 18-26.

Bässler, U. (1983). *Neural Basis of Elementary Behavior in Stick Insects*. Berlin, Heidelberg, New York: Springer.

Bässler, U. (1993). The femur-tibia control system of stick insects – a model system for the study of the neural basis of joint control. *Brain Res. Rev.* **18**, 207-226.

Bässler, U. and Büschges, A. (1998). Pattern generation for stick insect walking movements – multisensory control of a locomotor program. *Brain Res. Rev.* **27**, 65-88.

Bässler, U. and Stein, W. (1996). Contributions of structure and innervation pattern of the stick insect extensor tibiae muscle to the filter characteristics of the muscle–joint system. *J. Exp. Biol.* **199**, 2185-2198.

Bässler, U. and Storrer, J. (1980). The neural basis of the femur-tibia-control-system in the stick insect *Carausius morosus*. I. Motoneurons of the extensor tibiae muscle. *Biol. Cybern.* **38**, 107-114.

Bässler, D., Büschges, A., Meditz, S. and Bässler, U. (1996). Correlation between muscle structure and filter characteristics of the muscle–joint system in three orthopteran insect species. *J. Exp. Biol.* **199**, 2169-2183.

Blickhan, R., Wagner, H. and Seyfarth, A. (2003). Brain or muscles. In *Recent Research Developments in Biomechanics.* Vol. 1 (ed. S. G. Pandalai), pp. 215-245. India: Transworld Research Network, Thiru-anantha-puram (Trivandrum).

Brezina, V. and Weiss, K. R. (2000). The neuromuscular transform constrains the production of functional rhythmic behaviors. *J. Neurophysiol.* **83**, 232-259.

Brezina, V., Orekhova, I. V. and Weiss, K. R. (2000). The neuromuscular transform: the dynamic, nonlinear link between motor neuron firing patterns and muscle contraction in rhythmic behaviors. *J. Neurophysiol.* **83**, 207-231.

Brown, I. E. and Loeb, G. E. (1999). Measured and modeled properties of mammalian skeletal muscle. I. The effects of post-activation potentiation on the time-course and velocity dependencies of force production. *J. Muscle Res. Cell Motil.* **20**, 443-456.

Brown, I. E., Cheng, E. J. and Loeb, G. E. (1999). Measured and modeled properties of mammalian skeletal muscle. II. The effects of stimulus frequency on force-length and force-velocity relationships. *J. Muscle Res. Cell Motil.* **20**, 627-643.

Burns, M. D. and Usherwood, P. N. R. (1978). Mechanical properties of locust extensor tibiae muscles. *Comp. Biochem. Physiol.* **61A**, 85-95.

Büschges, A. (1995). Role of local nonspiking interneurons in the generation of rhythmic motor activity in the stick insect. *J. Neurobiol.* **27**, 488-512.

Büschges, A. (2005). Sensory control and organization of neural networks mediating coordination of multisegmental organs for locomotion. *J. Neurophysiol.* **93**, 1127-1135.

Büschges, A., Kittmann, R. and Schmitz, J. (1994). Identified nonspiking interneurons in leg reflexes and during walking in the stick insect. *J. Comp. Physiol. A* **174**, 685-700.

Büschges, A., Ludwar, B. C., Bucher, D., Schmidt, J. and DiCaprio, R.

(2004). Synaptic drive contributing to rhythmic activation of motoneurons in the deafferented stick insect walking system. *Eur. J. Neurosci.* **19**, 1856-1862.

Chiel, H. J. and Beer, R. D. (1997). The brain has a body: adaptive behavior emerges from interactions of nervous system, body and environment. *Trends Neurosci*. **20**, 553-557.

Cruse, H. and Bartling, C. (1995). Movement of joint angles in the legs of a walking insect *Carausius morosus*. *J. Insect Physiol.* **41**, 761-771.

Debrodt, B. (1980). Untersuchungen über die Innervation des Flexor tibiae an *Carausius morosus*. Diplomarbeit, University of Kaiserslautern, Germany.

Debrodt, B. and Bässler, U. (1989). Motor neurones of the flexor tibiae muscle in phasmids. *Zool. Jb. Physiol*. **93**, 481-494.

Debrodt, B. and Bässler, U. (1990). Responses of flexor motor neurons to stimulation of the femoral chordotonal organ of the phasmid *Extrasoma tiaratum*. *Zool. Jb. Physiol*. **94**, 101-119.

De Haan, A. (1998). The influence of stimulation frequency on force-velocity characteristics of in situ rat medial gastrocnemius muscle. *J. Exp. Physiol.* **83**, 77-84.

Dixon, W. J. and Massey, F. J. (1969). *Introduction to Statistical Analysis*. New York: McGraw Hill.

Driesang, R. B. and Büschges, A. (1996). Physiological changes in central neuronal path-ways contributing to the generation of a reflex reversal. *J. Comp. Physiol. A* **179**, 45-57.

Dürr, V., Schmitz, J. and Cruse, H. (2004). Behaviour-based modelling of hexapod locomotion: linking biology and technical application. *Arthropod Struct. Dev.* **33**, 237-250.

Edman, K. A. P. (1979). The velocity of unloaded shortening and its relation to sarcomere length and isometric force in vertebrate muscle fibres. *J. Physiol*. **291**, 143-159.

Edman, K. A. P. (1988). Double-hyperbolic force-velocity relation in frog muscle fibres. *J. Physiol.* **404**, 301-321.

Edman, K. A. P. and Curtin, N. A. (2001). Synchronous oscillations of length and stiffness during loaded shortening of frog muscle fibres. *J. Physiol.* **534**, 553-563.

Edman, K. A. P., Mulieri, L. A. and Scubon-Mulieri, B. (1976). Non-hyperbolic force-velocity relationship in single muscle fibres. *Acta Physiol. Scand.* **98**, 143-156.

Edman, K. A. P., Elzinga, G. and Noble, M. I. M. (1978). Enhancement of mechanical performance by stretch during tetanal contractions of vertebrate skeletal muscle fibres. *J. Physiol.* **281**, 139-155.

Ekeberg, Ö., Blümel, M. and Büschges, A. (2004). Dynamic simulation of insect walking. *Arthropod Struct. Dev.* **33**, 287-300.

Fischer, H., Schmidt, J., Haas, R. and Büschges, A. (2001). Pattern generation for walking and searching movements of a stick insect leg II. Control of motoneuronal activity. *J. Neurophysiol.* **85**, 341-353.

Friedrich, H. (1932). Nervenphysiologische Studien an Insekten I. Untersuchungen über das reizphysiologische Verhalten der Extremitäten von *Dixippus morosus. Z. Vergl. Physiol*. **18**, 536-561.

Full, R. J. (1997). Invertebrate locomotor systems. In *The Handbook of Comparative Physiology* (ed. W. Dantzler), pp. 853-930. Oxford: Oxford University Press.

Full, R. J. and Ahn, A. N. (1995). Static forces and moments generated in the insect leg: comparison of a three-dimensional musculo-skeletal computer model with experimental measurements. *J. Exp. Biol.* **198**, 1285-1298.

Full, R. J., Stokes, D. R., Ahn, A. N. and Josephson, R. K. (1998). Energy absorption during running by leg muscles in a cockroach. *J. Exp. Biol.* **201**, 997-1012.

Gabriel, J. P., Scharstein, H., Schmidt, J. and Büschges, A. (2003). Control of flexor moto-neuron activity during single leg walking of the stick insect on an electronically controlled treadwheel. *J. Neurobiol*. **56**, 237-251.

Gordon, A. M., Huxley, A. F. and Julian, F. J. (1966). The variation in isometric tension with sarcomere length in vertabrate muscle fibres. *J. Physiol.* **184**, 170-192.

Graham, D. (1985). Pattern and control of walking in insects. *Adv. Insect Physiol.* **18**, 131-140.

Hildebrand, M. (1988). *Analysis of Vertebrate Structure*. New York, Toronto: John Wiley & Sons.

Hill, A. V. (1938). The heat of shortening and the dynamic constants of muscle. *Proc. R. Soc. Lond. B Biol. Sci.* **126**, 136-195.

Hooper, S. L. and Weaver, A. L. (2000). Motor neuron activity is often insufficient to predict motor response. *Curr. Opin. Neurobiol.* **10**, 676-682.

Hooper, S. L., Guschlbauer, C., von Uckermann, G. and Büschges, A. (2006). Natural neural output that produces highly variable locomotory movements. *J. Neurophysiol.* **96**, 2072-2088.

Hooper, S. L., Guschlbauer, C., von Uckermann, G. and Büschges, A. (2007). Different motor neuron spike patterns produce contractions with very similar rises in graded slow muscles. *J. Neurophysiol.* **97**, 1428-1444.

Jewell, B. R. and Wilkie, D. R. (1958). An analysis of the mechanical components in frog striated muscle. *J. Physiol.* **143**, 515-540.

Josephson, R. K. (1985). Mechanical power output from striated muscle during cyclic contraction. *J. Exp. Biol.* **114**, 493-512.

Josephson, R. K. (1993). Contraction dynamics and power output of skeletal muscle. *Annu. Rev. Physiol*. **55**, 527-546.

Karg, G., Breutel, G. and Bässler, U. (1991). Sensory influences on the coordination of two leg joints during searching movements of stick insects. *Biol. Cybern*. **64**, 329-335.

Kittmann, R., Schmitz, J. and Büschges, A. (1996). Premotor interneurons in generation of adaptive leg reflexes and voluntary movements in stick insects. *J. Neurobiol.* **31**, 512-531.

Malamud, J. G. (1988). The effects of octopamine on contraction kinetics and power output of a locust flight muscle. *J. Comp. Physiol.* **162**, 827-835.

Malamud, J. G. (1989). The tension in a locust flight muscle at varied muscle lengths. *J. Exp. Biol.* **144**, 479-494.

Malamud, J. G. and Josephson, R. K. (1991). Force–velocity relationships of a locust flight muscle at different times during a twitch contraction. *J. Exp. Biol.* **159**, 65-87.

Marquardt, F. (1940). Beiträge zur Anatomie der Muskulatur und der peripheren Nerven von *Carausius* (*Dixippus*) *morosus*. *Zool. Jb. Abt. Ont. Tiere* **66**, 63-128.

Meyrand, P. and Marder, E. (1991). Matching neural and muscle oscillators: control by FMRFamide-like peptides. *J. Neurosci.* **11**, 1150-1161.

Morris, L. G. and Hooper, S. L. (1997). Muscle response to changing neuronal input in the lobster (*Panulirus interruptus*) stomatogastric system: spike number- *versus* spike frequency-dependent domains. *J. Neurosci*. **17**, 5956-5971.

Morris, L. G., Thuma, J. B. and Hooper, S. L. (2000). Muscles express motor patterns of non-innervating neural networks by filtering broad-band input. *Nat. Neurosci.* **3**, 245-250.

Orlovsky, G. N., Deliagina, T. G. and Grillner, S. (1999). *Neuronal Control of Locomotion*. Oxford: Oxford University Press.

Rack, P. M. and Westbury, D. R. (1969). The effects of length and stimulus rate on tension in the isometric cat soleus muscle. *J. Physiol.* **204**, 443-460.

Schmitz, J. and Hassfeld, G. (1989). The treading-on-tarsus reflex in stick insects: phase dependence and modifications of the motor output during walking. *J. Exp. Biol*. **143**, 373-388.

Siebert, T., Wagner, H. and Blickhan, R. (2003). Not all oscillations are rubbish: forward simulation of quick-release experiments. *J. Mech. Med. Biol.* **3**, 107-122.

Stephenson, D. G. and Wendt, I. R. (1984). Length dependence in sarcoplasmic calcium concentration and myofibrillar calcium sensitivity in striated muscle fibres. *J. Muscle Res. Cell Motil.* **5**, 243-272.

Stevenson, R. D. and Josephson, R. K. (1990). Effects of operating frequency and temperature on mechanical power output from moth flight muscle. *J. Exp. Biol.* **149**, 61-78.

Storrer, J. (1976). Systemanalytische Untersuchungen am 'Kniesehnenreflex' der Stabheuschrecke Carausius morosus Br. (Orthoptera). Thesis/ dissertation, Fachbereich Biologie der Universität Kaiserslautern, Germany, pp. 6-119.

Storrer, J., Bässler, U. and Mayer, S. (1986). Motoneurone im Meso- und Metathorakalganglion der Stabheuschrecke *Carausius morosus*. *Zool. Jb. Physiol*. **90**, 359-374.

Thorson, J. and Biedermann-Thorson, M. (1974). Distributed relaxation processes in sensory adaptation. *Science* **183**, 161-172.

Watson, A. H. D. and Pflüger, H.-J. (1994). Distribution of input synapses from processes exhibiting GABA- and glutamate-like immunoreactivity onto terminals of prosternal filiform afferents in the locust. *J. Comp. Neurol*. **343**, 617-629.

Weidler, D. J. and Diecke, F. P. J. (1969). The role of cations in conduction in the central nervous system of the herbivorous insect *Carausius morosus*. *Z. Vergl. Physiol*. **64**, 372-399.

White, D. C. S. (1977). Muscle mechanics. In *Mechanics and Energetics of Animal Locomotion* (ed. R. McN. Alexander and G. Goldspink), pp. 23-55. New York: John Wiley & Sons.

Wilkie, D. R. (1956). Measurement of the series elastic component at various times during a single muscle twitch. *J. Physiol.* **134**, 527-530.